Progress In Electromagnetics Research, Vol. 119, 107–132, 2011

A NOVEL APPROACH TO TARGET LOCALIZATION THROUGH UNKNOWN WALLS FOR THROUGH-THE-WALL RADAR IMAGING

Y. Jia*, L. J. Kong, and X. B. Yang

School of Electronic Engineering, University of Electronic Science and Technology of China, Chengdu, Sichuan 611731, China

Abstract—This paper mainly deals with the problem of target localization with unknown wall parameters for through-the-wall radar imaging (TWRI) applications. A novel approach is presented to correct the shift in target position due to the ambiguities of the wall parameters. This approach is based on imaging by using at least two assumed wall relative permittivities. For each assumed relative permittivity, a sequence of target images are obtained using different assumed wall thicknesses, and a linear trajectory is formed via Radon transform. The intersection of these linear trajectories corresponding to different assumed relative permittivities is the estimated target position. Besides, the estimated wall parameters are acquired to form the high-quality image. Simulation and experiment results show that the estimated target positions with the proposed approach are well consistent with the true target locations, and the high-quality images are generated with the estimated wall parameters.

1. INTRODUCTION

Through-the-Wall Radar Imaging (TWRI) is considered as a useful tool to image the scene behind the obstacles, such as walls, snow, rubbles and other visually opaque materials. Therefore, TWRI is widely used in both military and commercial spheres, such as rescue missions, surveillance and anti-terrorism. Nowadays, the main studies on TWRI are to detect and track humans behind walls with known wall parameters, such as wall thickness and relative permittivity [1–10]. In the previous work, we have researched TWRI with known wall parameters [11, 12]. However, in practical situations, the wall

Received 24 May 2011, Accepted 1 July 2011, Scheduled 21 July 2011

* Corresponding author: Yong Jia (jiayong920@gmail.com).

parameters are not known exactly. Ambiguities in wall parameters defocus and blur target image, and displace target away from its true position. Therefore, it is difficult to implement accurate TWRI to obtain the high-quality image without the defocusing of target image and target displacement.

To implement accurate TWRI with unknown wall parameters, the basic method is to precisely estimate wall parameters and then to form the image with the estimated wall parameters. Based on the single-layer and homogeneous wall model and the Fresnel equations of plane wave propagation, an effective and fast algorithm for wall parameters estimation that can be used in practice was presented in [13], which was implemented with the extraction for the magnitudes and the time positions of reflections from inner and outer interfaces of the wall. However, in this algorithm, the bistatic antennas are desired to move towards the wall in order to reduce the unwanted clutter (the echoes of ceiling, floor, back wall etc.). Due to the refraction in the interface between wall and air, the setup of bistatic antennas results in that the propagation time within the wall changes along with the antennas moving. Therefore, the time position of the reflection from inner interface of the wall is coupled with error through averaging all the echo impulses, which introduces error in the estimated wall thickness to decrease the accuracy of TWRI.

There are some other approaches to implement accurate TWRI through correcting the defocusing of target image or the target displacement with wall parameters estimation in the single-layer and homogeneous wall model. The degree of defocusing and blurring of target image was studied and corrected by applying auto-focusing metrics [14–16]. The target displacement owing to wall parameter errors was discussed and two techniques were proposed by Wang et al. in [17, 18]. The two techniques require that the data must be acquired under at least two different setups of antenna array. For each array setup, with one assumed relative permittivity, the displacements of imaged target position due to different assumed wall thicknesses form a linear trajectory. The cross point of two trajectories, corresponding to the two array structures or two standoff distances, is regarded as the estimated target position. Then the estimated wall parameters are obtained by the estimated target position, which can be applied to form the high-quality image. In practical applications, however, antenna position errors will be introduced by changing the setup of antenna array, which lowers the localization accuracy and the image quality. Besides, taking the safety of operator into consideration, the TWRI system may not be allowed to work at two array setups by manual operation. For example, in the anti-terrorism, changing the

array setups by manual operation of operator will make some noise, which will draw the attention of terrorists hiding in room to threaten the safety of operator.

Inspired by the works in [17, 18], a novel approach to target localization in the presence of wall parameter ambiguities for TWRI is presented with the single-layer and homogeneous wall model in this paper. Under the condition of the fixed antenna array, the approach is based on imaging by using at least two assumed wall relative permittivities. For each assumed relative permittivity, target positions form a linear trajectory with different assumed wall thicknesses. The target position is estimated by the intersection of these linear trajectories with different assumed relative permittivities. Besides, the wall parameters are estimated to generate the high-quality image. So compared with the two techniques in [17, 18], the approach with fixed setup of antenna array can improve the potential localization accuracy and image quality, and ensure the operator's safety without manual operation in real applications. Besides, Radon transform is used to obtain the linear trajectory, which counteracts the negative effect of image defocusing effectively. Finally, a simulation example is provided to demonstrate the effectiveness of the proposed approach, and a TWRI experiment is implemented to test and verify the approach by using aperture synthesis technique in practical environment.

The rest of this paper is organized as follows. We provide in Section 2 the basic theory and equations of through-the-wall back-projection imaging. The novel target localization approach is proposed in Section 3. In Section 4, the simulation results are provided. The TWRI experiment results are presented in Section 5. Finally the conclusion is provided in Section 6.

2. FUNDAMENTALS OF THROUGH-THE-WALL IMAGING

In this section, the back-projection imaging process through unknown walls for the proposed antenna setup is discussed primarily. A single transmitter and a single receiver are used to synthesize an M-element transceiver linear array. The mth transmitter, located at $X_{t_m} = (x_{t_m}, y_{t_m})$, illuminates the scene with a wideband signal $s(t)$. The mth receiver, only receiving the echo signal from the mth transmitter, is located at $X_{r_m} = (x_{r_m}, y_{r_m})$. For a single point target p at $X_p = (x_p, y_p)$, the output of the mth receiver is given by

$$y_m(X_p) = a(X_p)s(t - \tau_{p,m}) \tag{1}$$

where $a(X_p)$ is the complex reflectivity of the point target.

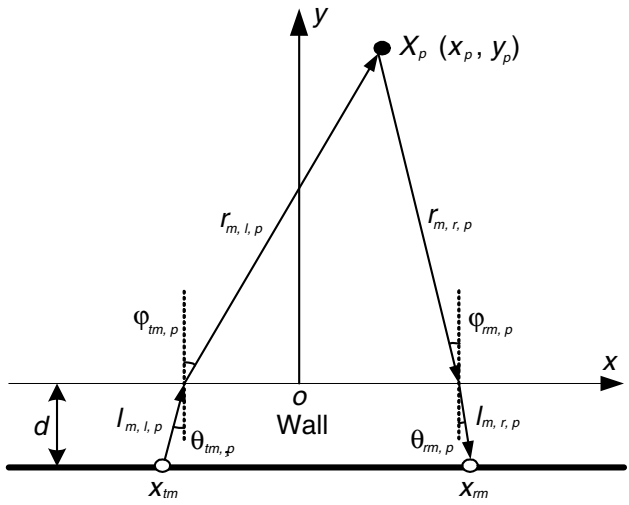

Figure 1. Geometry for computing the distance on transmitter and receiver.

As shown in Figure 1, on the basis of the single-layer and homogeneous wall model, the propagation delay $\tau_{p,m}$ can be given by

$$\tau_{p,m} = \frac{r_{m,t,p} + r_{m,r,p}}{c} + \frac{l_{m,t,p} + l_{m,r,p}}{v} \tag{2}$$

where c and v are the propagation speeds in the air and in the wall respectively. v is given by $v = c/\sqrt{\varepsilon}$, associating solely with wall relative permittivity.

Figure 2 shows the block diagram of the imaging system. For a single target case, the system output, namely, the value of the pixel q located at $X_q = (x_q, y_q)$, is given by

$$I(X_q) = \sum_{m=1}^{M} a(X_p) s\left(t - \tau_{p,m} + \tau_{q,m}\right)|_{t=0} \tag{3}$$

where the focusing delay $\tau_{q,m}$ is applied to the output of the mth receiver when the transmitter is at the mth location, which is the same as the propagation delay $\tau_{p,m}$ except that the target p is replaced by the focusing pixel q. The focusing delay $\tau_{q,m}$ can be precisely computed with exact wall parameters by Snell's law [2]. Note that the pixel value $I(X_q)$ depends on the shape of the signal with the maximum value in $t = 0$.

The process described by (3) is performed for all pixels in the region of interest to generate the composite image of the scene. The

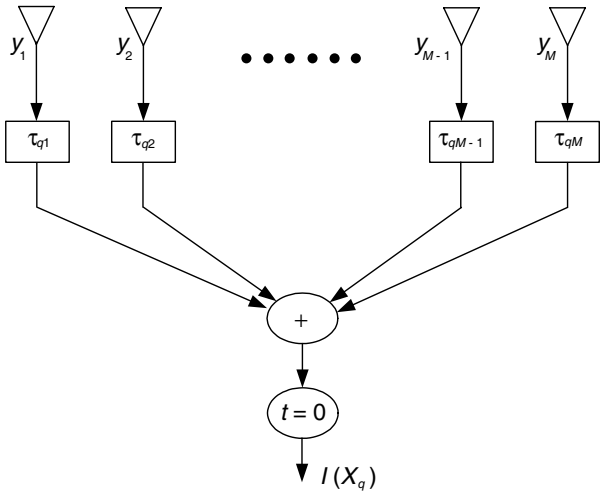

Figure 2. Block diagram of the imaging process.

general case of multiple targets can be obtained by superposition of target reflections.

3. NOVEL TARGET LOCALIZATION APPROACH THROUGH UNKNOWN WALLS

In practical situations, the wall parameters, namely, wall thickness and relative permittivity, are not exactly known. According to the fundamentals of through-the-wall imaging in Section 2, the estimated errors of wall parameters impact the traveling time both inside and outside the wall, and subsequently lead to corresponding errors in the focusing delay $\tau_{q,m}$ for coherent imaging. Finally, the effect defocus and blur the target images, and shift the imaged targets' positions away from their true positions.

In this paper, the target displacement in imaging results caused by wall parameter errors is studied primarily. The effect of relative permittivity error on target localization is not as sensitive as that of wall thickness error [17]. Thus, we mainly analyze the target displacement due to wall thickness error in the following, and then a novel target localization approach is presented.

3.1. Target Displacement Due to Wall Thickness Error

Firstly, we define the assumed wall thickness and relative permittivity are (d_e, ε_e) which in general are not equal to the true wall parameters

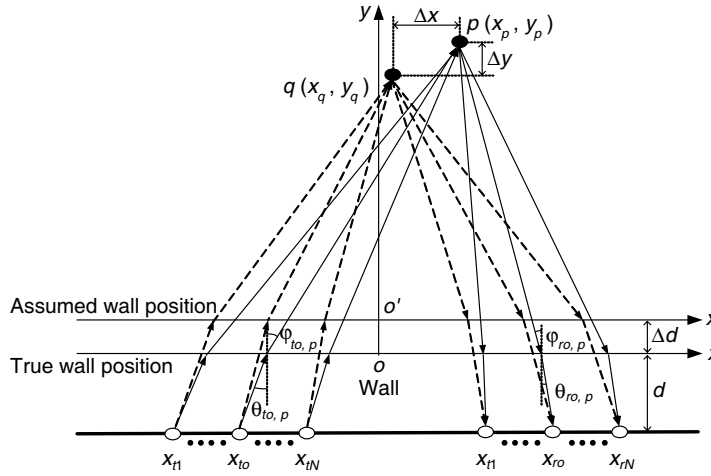

Figure 3. Geometry for computing the target displacement caused by thickness error Δd.

(d_T, ε_T). Suppose the errors are Δd and $\Delta\varepsilon$. Thus, the assumed wall parameters (d_e, ε_e) are denoted as $d_e = d_T + \Delta d$ and $\varepsilon_e = \varepsilon_T + \Delta\varepsilon$.

As shown in Figure 3, the target appears at point p with the wall parameters (d_T, ε_e). Due to the thickness error Δd, the target is shifted from point p to point q. Thus, point q is the target position with the parameters $(d_T + \Delta d, \varepsilon_e)$. Besides, $\Delta x_{pq} = x_q - x_p$ and $\Delta y_{pq} = y_q - y_p$ are used to denote the displacement. According to the conclusion in [17, 18], after replacing ε by ε_e, Δx_{pq} and Δy_{pq} are written as

$$\Delta x_{pq} = -\Delta d(\varepsilon_e - 1)\left[\tan(\theta_{to,p}) + \tan(\theta_{ro,p})\right] \tag{4}$$

$$\Delta y_{pq} = -\Delta d\left[\frac{\cos(\varphi_{to,p})}{\cos(\theta_{to,p})}\sqrt{\varepsilon_e} + \frac{\cos(\varphi_{ro,p})}{\cos(\theta_{ro,p})}\sqrt{\varepsilon_e} - 2\right] \tag{5}$$

where $\theta_{to,p}$ and $\varphi_{to,p}$, referring to Figure 3, are the incident and refraction angles in the wall and air, related to the path from the center (x_{to}, y_{to}) of transmitting antenna array to point p respectively. Accordingly, $\theta_{ro,p}$ and $\varphi_{ro,p}$ are, separately, the incident and refraction angle in the wall and air, related to the path from point p to the center (x_{ro}, y_{ro}) of receiving antenna array. Note that (4) and (5) are derived based on two conditions. First, the array aperture is small. Second, the delay difference $\Delta\tau_{pq,o} = \tau_{p,o} - \tau_{q,o}$ is identically equal to zero for different assumed relative permittivities $\varepsilon_e s$, where $\tau_{p,o}$ and $\tau_{q,o}$ are the time delays respectively corresponding to the paths $(x_{to}, y_{to}) \to p \to (x_{ro}, y_{ro})$ and $(x_{to}, y_{to}) \to q \to (x_{ro}, y_{ro})$.

3.2. Principle of the Target Localization Approach

Based on (4) and (5), target position is linear with the wall thickness for the assumed relative permittivity ε_e. Along with the changing of wall thickness, target positions form a linear trajectory. Slope k of the linear trajectory is given by

$$k = \frac{\Delta y_{pq}}{\Delta x_{pq}} = \frac{\left[\frac{\cos(\varphi_{to,p})}{\cos(\theta_{to,p})}\sqrt{\varepsilon_e} + \frac{\cos(\varphi_{ro,p})}{\cos(\theta_{ro,p})}\sqrt{\varepsilon_e} - 2\right]}{(\varepsilon_e - 1)\left[\tan(\theta_{to,p}) + \tan(\theta_{ro,p})\right]} \tag{6}$$

Therefore, the slope k of linear trajectory is a function of the assumed relative permittivity ε_e and the angles $\theta_{to,p}$, $\varphi_{to,p}$, $\theta_{ro,p}$, $\varphi_{ro,p}$ related to the path between point p and array center (x_{to}, y_{to}), (x_{ro}, y_{ro}). Furthermore, $\theta_{to,p}$, $\varphi_{to,p}$, $\theta_{ro,p}$, $\varphi_{ro,p}$ are determined by the setup of antenna array and assumed relative permittivity under the true wall thickness, which can be expressed as

$$\begin{cases} [\theta_{to,p},\, \varphi_{to,p}] = f_t\,(x_{to},\, y_{to},\, \varepsilon_e) \\ [\theta_{ro,p},\, \varphi_{ro,p}] = f_r\,(x_{ro},\, y_{ro},\, \varepsilon_e) \end{cases} \tag{7}$$

$$\begin{cases} (x_{to},\, y_{to}) = \frac{1}{M}\left(\sum\limits_{m=1}^{M} x_{tm},\, \sum\limits_{m=1}^{M} y_{tm}\right) \\ (x_{ro},\, y_{ro}) = \frac{1}{M}\left(\sum\limits_{m=1}^{M} x_{rm},\, \sum\limits_{m=1}^{M} y_{rm}\right) \end{cases} \tag{8}$$

where (x_{tm}, y_{tm}) and (x_{rm}, y_{rm}) are the coordinates of the transmitting and receiving antenna array, respectively, which represent the setup of antenna array.

Thus, the function of the slope k is expressed as

$$k = f(\varepsilon_e,\, x_{tm},\, y_{tm},\, x_{rm},\, y_{rm}) \tag{9}$$

From (9), we obtain the conclusion that the slope k of linear target trajectory is determined by the assumed relative permittivity ε_e and the setup of antenna array (x_{tm}, y_{tm}), (x_{rm}, y_{rm}).

Based on the above conclusion, with one fixed setup of antenna array, the slope of linear target trajectory caused by changing wall thickness is uniquely determined by the assumed relative permittivity ε_e. Therefore, the proposed approach requires imaging to be performed under at least two assumed relative permittivities $\varepsilon_e s$ for one fixed setup of antenna array. For each ε_e, target positions form a linear trajectory by using different assumed wall thicknesses $d_e s$. The slope of the linear trajectory is related to ε_e alone. Consequently, there are different linear trajectories with different slopes corresponding to different $\varepsilon_e s$. Moreover, all these trajectories cross over the true target position, because the target displacement due to the error in each

assumed relative permittivity and that due to wall thickness error are canceled with each other. That is to say, the common cross point of these trajectories is the true target position. So the cross point of these trajectories is taken as the estimation of true target location.

Furthermore, for each assumed relative permittivity ε_e, the relationship of wall thickness d and target position (x, y) can be obtained from (4) and (5) as

$$\begin{cases} d = A'x + B' \\ d = Ay + B \end{cases} \tag{10}$$

Then the estimation $\hat{d}$ of wall thickness is found by substituting the estimated target position $(\hat{x}, \hat{y})$ for (x, y) in (10). As a result, the estimated wall parameters $(\hat{\varepsilon}, \hat{d}) = (\varepsilon_e, \hat{d})$ are acquired to form the final image. Note that the estimated wall thickness $\hat{d}$ depends on the assumed relative permittivity ε_e. Therefore, multiple pairs $(\varepsilon_e, \hat{d})$ are obtained to generate the final image.

3.3. Processing Flow of the Target Localization Approach

Below, we give an exhaustive processing flow of the target localization algorithm under unknown wall parameters.

(1) For an assumed relative permittivity ε_{e1},
- Generate a sequence of images $A_{d_{e1}}, A_{d_{e2}}, \ldots, A_{d_{eK}}$ with the assumed wall thicknesses $d_{e1}, d_{e2}, \ldots, d_{eK}$.
- Find the target position $I_1(x, y, d_{el})$ in image $A_{d_{el}}$ for $l = 1, 2, \ldots, K$ by two-dimension sliding window detection, and fit $I_1(x, y, d_{el})$ with $d = A_1 y + B_1$ via least-square fitting, where d represents the variable of wall thickness.
- Fit the image sequence $A_{d_{e1}}, A_{d_{e2}}, \ldots, A_{d_{eK}}$ with a linear trajectory expressed as $y = k_1 x + b_1$ by using Radon transform.

(2) Change the relative permittivity to $\varepsilon_{e2}, \varepsilon_{e3}, \ldots, \varepsilon_{eN}$ and repeat step 1 to generate corresponding linear trajectories $y = k_2 x + b_2$, $y = k_3 x + b_3, \ldots, y = k_N x + b_N$ and polynomials $d = A_2 y + B_2$, $d = A_3 y + B3, \ldots, d = A_N y + B_N$.

(3) Select two linear trajectories $y = k_i x + b_i$, $y = k_j x + b_j$, $i, j = 1, 2, \ldots, N, i \neq j$ arbitrarily to find their cross point. Finally, C_N^2 cross points expressed as (x_n, y_n), $n = 1, 2, \ldots, C_N^2$ are obtained.

(4) Use $(\hat{x}, \hat{y}) = (\sum x_n / C_N^2, \sum y_n / C_N^2)$, $n = 1, 2, \ldots, C_N^2$ as the estimation of the true target location.

(5) Put $\hat{y}$ into $y = k_i x + b_i$ to find $\bar{x}_i$ and calculate the difference $\Delta x_i = |\bar{x}_i - \hat{x}|$, $i = 1, 2, \ldots, N$.

(6) Find the minimum $\Delta x_{\min}$ in $\Delta x_i, i = 1, 2, \ldots, N$, and the corresponding relative permittivity ε_e of $y = kx + b$ for $\Delta x_{\min}$ is used as the estimation $\hat{\varepsilon}$ of wall relative permittivity.

(7) Put $\hat{y}$ into $d = Ay + B$ corresponding to $\hat{\varepsilon}$ to find the estimation $\hat{d} = A\hat{y} + B$ of wall thickness.

(8) Use the estimated wall parameters $(\hat{\varepsilon}, \hat{d})$ to generate the final image.

The above processing flow deserves five comments.

(i) Because the errors of wall parameters smear and defocus the target image, there are errors in these detected target locations $I(x, y, d_{el})$, $l = 1, 2, \ldots, K$ in step 1. According to the simulation and experiment results, the error in target x-coordinate is usually larger than in target y-coordinate. Therefore, the first-order polynomial $d = Ay + B$ is obtained by fitting the wall thickness and target y-coordinate in step 2, which can be used to find comparatively accurate estimation $\hat{d} = A\hat{y} + B$ of wall thickness in step 7.

(ii) Due to the inaccuracy of these target locations $I(x, y, d_{el})$, $l = 1, 2, \ldots, K$, it is impossible to obtain an accurate linear trajectory by fitting these target locations. It is well known that Radon transform is widely used in detecting line in image domain. Thus, we use Radon transform to fit the sequence of target images with a linear trajectory in step 1. Moreover, Radon transform used in image domain reduces the effect of target size to a certain extent.

(iii) Theoretically, all these linear trajectories $y = k_i x + b_i$, $i = 1, 2, \ldots, N$ cross over the target true position. Thereby each of the cross points (x_n, y_n), $n = 1, 2, \ldots, C_N^2$ in step 3 can be the estimated target position. In practical situations, however, because of target image smearing and defocusing, there are still deviations in these trajectories fitted by Radon transform, which causes worse fluctuation in these cross points. To overcome the fluctuation, in step 4, the statistical mean $(\hat{x}, \hat{y})$ of these cross points is used as the effective estimation of target position.

(iv) According to the simulation result in Figure 5, the slope of target displacement trajectory changes little with the variety of relative permittivity, which is adverse in fitting with linear trajectory. So, generally, the minimal difference between the assumed relative permittivities should be larger than 2, namely, $|\varepsilon_{ei} - \varepsilon_{ej}| \geq 2$, $(i, j = 1, 2, \ldots, N, i \neq j)$. With the typical construction of

practical walls, the range of the assumed wall relative permittivity lies from 4 to 16. Therefore, the number N is smaller than 8, that is, $2 \leq N \leq 7$.

(v) Based on the typical construction of practical walls, the assumed wall thickness d_e is limited within the range from 0.1 m to 0.5 m. The number K of the assumed wall thicknesses should be properly chosen to obtain an accurate linear trajectory by Radon transform. This is because that a small K is not enough to be fitted with a linear trajectory, while a large K introduces large errors in wall thickness, which reduces the accuracy of the fitted linear trajectory. Generally, the number K ranges from 5 to 10, namely, $5 \leq K \leq 10$.

4. SIMULATION RESULTS

In this section, a simulation is used to verify the proposed approach. The coordinate system in Figure 1 is used for the simulation and maintained throughout the paper. An amplitude modulated sinc pulse of 1 GHz bandwidth centered at 1.5 GHz with Gaussian noise is used for imaging, and the Signal-to-Noise ratio (SNR) of the range cells where targets exist is 8 dB. A 31-element linear array with 31 monostatic antennas is placed against the wall at positions listed in Table 1. The simulated wall is a 0.24 m thick, single-layer and homogeneous wall with relative permittivity $\varepsilon = 8.6$. The imaging scene $x \times y = [-3\,\text{m} \sim 3\,\text{m}] \times [0\,\text{m} \sim 6\,\text{m}]$ is divided into 256×256 pixel cells. One point target is placed at $(x, y) = (1.0\,\text{m}, 3.0\,\text{m})$ with the complex reflectivity $\alpha = 1$.

According to the processing flow, four assumed relative permittivities $\varepsilon_e = 6$, 9, 12, 15 are used to generate four sequences of target images, shown in Figure 4, with assumed thicknesses $d_e = 0.1$, 0.15, 0.2, 0.25, 0.3, 0.35, 0.4, 0.45, 0.5 m. Each target image sequence is the superposition of target images only preserving over 3 dB pixels. Figure 4(a) shows that the target image approaches to the center of antenna array to form an apparent linear trace with the addition of assumed wall thickness. Because of the defocusing of target images caused by the errors in wall parameters, there are three approximate linear traces in Figures 4(b), (c), (d). Besides, it is shown that all the four linear traces cross over the true target position.

Table 1. Monastatic antenna array locations.

Element ♯	1	2	3	...	29	30	31
Antenna locations (m)	−1.5	−1.4	−1.3	...	1.3	1.4	1.5

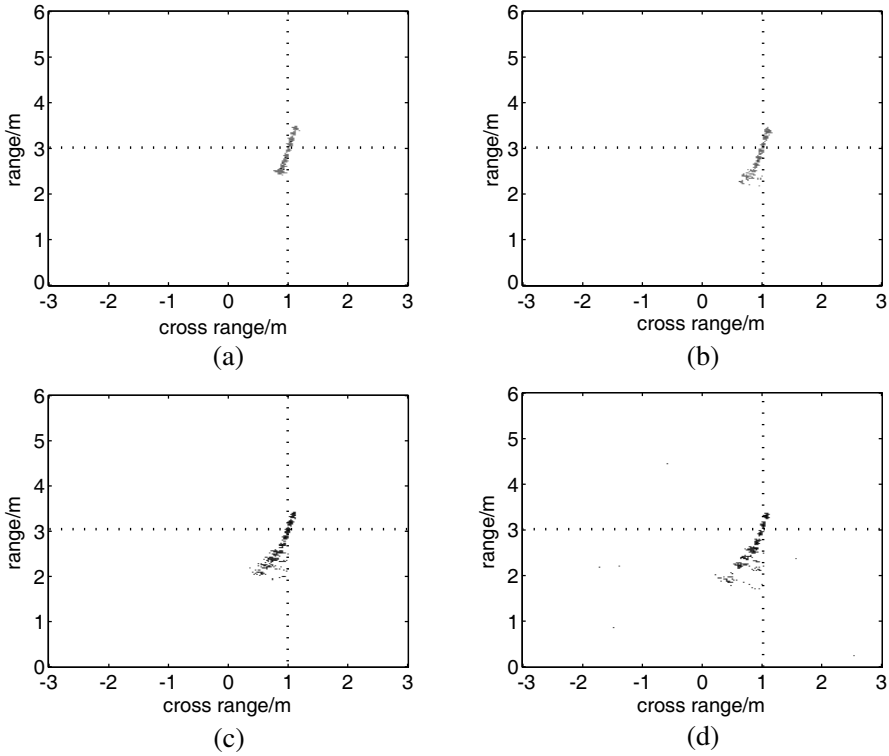

Figure 4. Image sequence of one target with $d_e = 0.1$, 0.15, 0.2, 0.25, 0.3, 0.35, 0.4, 0.45, 0.5 m for (a) $\varepsilon_e = 6$, (b) $\varepsilon_e = 9$, (c) $\varepsilon_e = 12$, (d) $\varepsilon_e = 15$.

Table 2. Cross points of four fitted lines in Figure 5.

Combination of two ε_e	Cross point (x, y) of two corresponding linear trajectories
$\varepsilon_e = 6$ and $\varepsilon_e = 9$	(1.02 m, 3.03 m)
$\varepsilon_e = 6$ and $\varepsilon_e = 12$	(1.01 m, 3.01 m)
$\varepsilon_e = 6$ and $\varepsilon_e = 15$	(1.01 m, 3.02 m)
$\varepsilon_e = 9$ and $\varepsilon_e = 12$	(0.98 m, 3.10 m)
$\varepsilon_e = 9$ and $\varepsilon_e = 15$	(0.98 m, 3.10 m)
$\varepsilon_e = 12$ and $\varepsilon_e = 15$	(0.97 m, 3.10 m)
statistical mean $(\hat{x}, \hat{y})$	(0.99 m, 3.06 m)

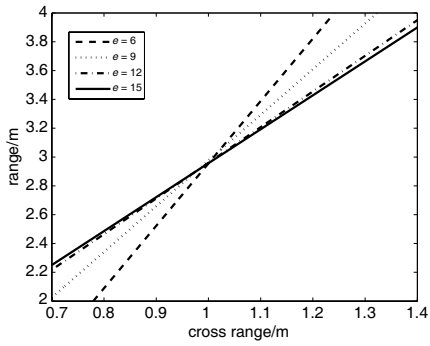

Figure 5. Four fitted lines with $\varepsilon_e = 6, 9, 12, 15$, $(\varepsilon_e = e)$.

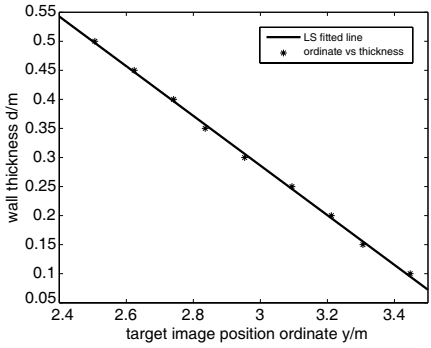

Figure 6. Least-square fitted polynomial with $\hat{\varepsilon} = 6$.

Figure 5 shows four fitted lines by fitting the four sequences of target images through Radon transform, and indicates that the slope of fitted line becomes small as the relative permittivity grows. The $C_4^2 = 6$ cross points of the four lines are listed in Table 2. Due to the errors in these fitted lines caused by image defocusing, some intersections, such as $(x_6, y_6) = (0.97\,\text{m}, 3.10\,\text{m})$, have larger localization errors. So the statistical mean $(\hat{x}, \hat{y}) = (0.99\,\text{m}, 3.06\,\text{m})$ of these cross points is regarded as the effective estimation of target position $(x, y) = (1.0\,\text{m}, 3.0\,\text{m})$.

By using the step 5 and step 6 of the processing flow, the estimation $\hat{\varepsilon} = 6$ of relative permittivity is selected from the four assumed relative permittivities $\varepsilon_e = 6, 9, 12, 15$, and the fitted first-order polynomial $d = A_1 y + B_1$ corresponding to $\hat{\varepsilon} = 6$ is shown in Figure 6. Then the estimated wall thickness $\hat{d} = 0.261\,\text{m}$ is found by $d = A_1\hat{y} + B_1$, $\hat{y} = 3.06$. The estimated wall parameters $(\hat{\varepsilon} = 6, \hat{d} = 0.261\,\text{m}) \neq (\varepsilon_T = 8.6, d_T = 0.24\,\text{m})$ are used to achieve the final image shown in Figure 7(a).

In order to demonstrate that the high-quality image can be formed by the estimated wall parameters with errors, the image with the true wall parameters is adopted as the comparison criterion, and two quantitative assessments are selected to estimate the image quality referring to the wall effects on TWRI. The first assessment is the displacement of target image given by

$$\Delta = \sqrt{(\tilde{x} - x)^2 + (\tilde{y} - y)^2} \tag{11}$$

where $(\tilde{x}, \tilde{y})$ is the position of target image and (x, y) is the true target position. The second assessment is the image contrast representing the defocusing and blurring of target image. The common measure for the

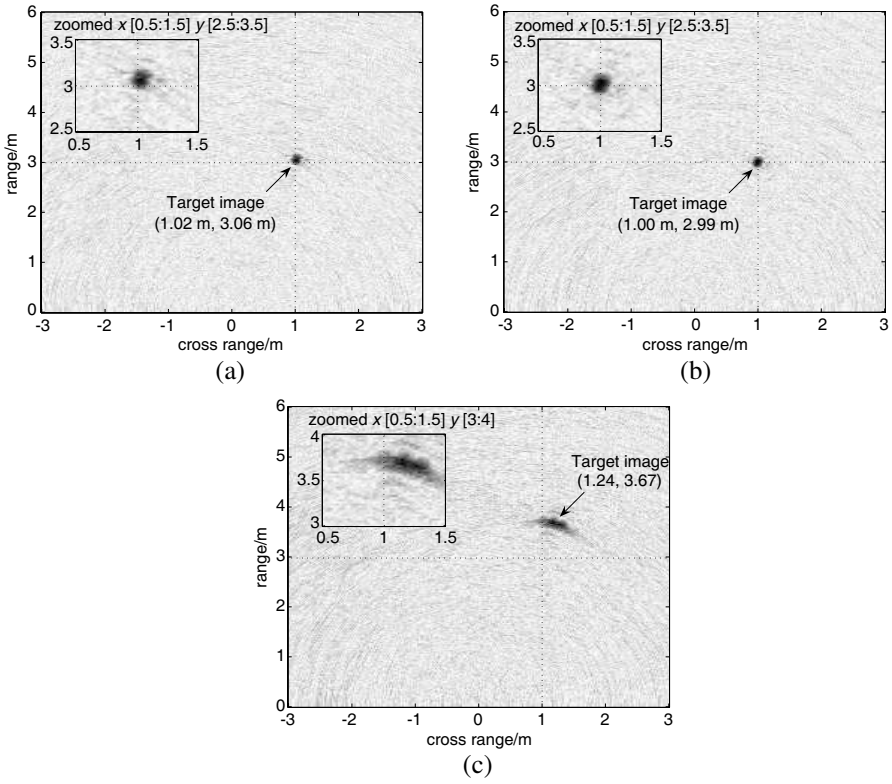

Figure 7. Imaging results with (a) $(\hat{\varepsilon}, \hat{d}) = (6,\ 0.261\,\text{m})$, (b) $(\varepsilon_T, d_T) = (8.6,\ 0.24\,\text{m})$, (c) $(\varepsilon, d) = (1,\ 0\,\text{m})$.

image contrast is the normalized sum of squared intensity (NSSI) [12] expressed as

$$\text{NSSI} = \frac{\sum_{q=1}^{Q} P(X_q)^4}{\left(\sum_{q=1}^{Q} P(X_q)\right)^4} \tag{12}$$

$$P(x_q) = \frac{|I(X_q)|}{\max\left(\{|I(X_q)|\}_{q=1}^{Q}\right)} \tag{13}$$

where $I(X_q)$ is the value of the pixel located at $X_q = (x_q, y_q)$ and Q is the number of the total image pixel.

With regard to Figure 7(a) with the estimated wall parameters $(\hat{\varepsilon}, \hat{d}) = (6, 0.261\,\text{m})$ and Figure 7(b) with the true wall parameters

(ε_T, d_T) = (8.6, 0.24 m), the positions of target images are successively estimated as (1.02 m, 3.06 m) and (1.00 m, 2.99 m) through two-dimension sliding window detection, which introduce the corresponding displacements 0.06 m and 0.01 m of target images according to (11), and the corresponding NSSIs are computed as 3.78×10^{-14} and 4.01×10^{-14} based on (12) and (13). Moreover, in practical application, TWRI is generally implemented without compensating wall effect when the wall parameters are not known a priori. Therefore, Figure 7(c) without wall compensation, namely with the wall parameters (ε, d) = (1, 0 m) is generated to be the additional comparison. It is clear that the serious defocusing and displacement of target image emerge in Figure 7(c) which has 0.71 m displacement of target image and 2.19×10^{-14} NSSI. In contrast to the three images in Figure 7, Figure 7(a) with the estimated wall parameters has the approximate displacement of target image and NSSI compared with Figure 7(b) with the true wall parameters, while it has major differences in the displacements of target images and NSSI compared with Figure 7(c) without wall compensation. Therefore, Figure 7(a) is judged as a high-quality image. It is demonstrated that although both two estimated wall parameters represent errors, they can be employed to form the high-quality image. This is because the effects of the estimated errors in wall thickness and relative permittivity are canceled out effectively, which efficiently corrects the set of focusing delays required to coherently combine the waveform returns from each pixel of the imaging scene. For simplicity of analysis, we omit to form the additional image without wall compensation in the following simulation and experiment.

To examine the feasibility of this localization approach in multiple targets, two point targets are located at (x, y) = (−1.0 m, 3.0 m) and (x, y) = (2.0 m, 1.0 m). Other simulation setups are maintained.

The same with the processing steps in one target, the image

Table 3. Cross points of the fitted lines for two targets.

Combination of two ε_e	Cross points (x, y) of the corresponding linear trajectories
$\varepsilon_e = 6$ and $\varepsilon_e = 9$	(−0.96 m, 2.94 m) (1.95 m, 1.01 m)
$\varepsilon_e = 6$ and $\varepsilon_e = 12$	(−0.97 m, 2.98 m) (2.01 m, 1.04 m)
$\varepsilon_e = 6$ and $\varepsilon_e = 15$	(−1.02 m, 3.06 m) (1.90 m, 0.98 m)
$\varepsilon_e = 9$ and $\varepsilon_e = 12$	(−1.02 m, 3.08 m) (2.04 m, 1.06 m)
$\varepsilon_e = 9$ and $\varepsilon_e = 15$	(−0.99 m, 3.01 m) (1.89 m, 0.97 m)
$\varepsilon_e = 12$ and $\varepsilon_e = 15$	(−1.01 m, 3.02 m) (1.81 m, 0.94 m)
statistical mean ($\hat{x}$, $\hat{y}$)	(−0.99 m, 3.01 m) (1.93 m, 1.00 m)

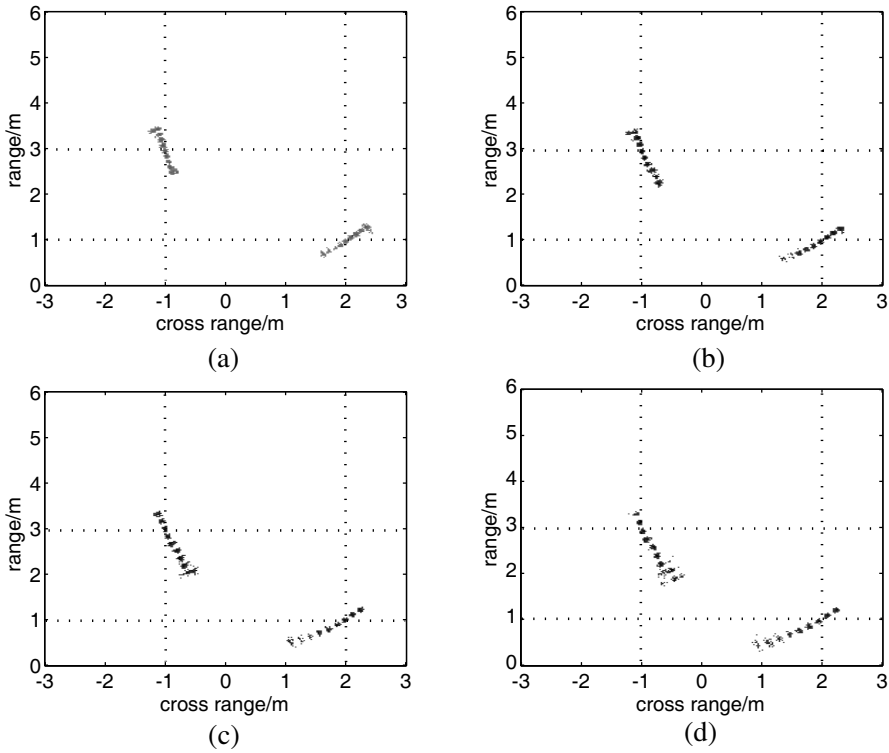

Figure 8. Image sequences of two targets with d_e = 0.1, 0.15, 0.2, 0.25, 0.3, 0.35, 0.4, 0.45, 0.5 m for (a) $\varepsilon_e = 6$, (b) $\varepsilon_e = 9$, (c) $\varepsilon_e = 12$, (d) $\varepsilon_e = 15$.

sequences of two targets, corresponding to each of the ε_e = 6, 9, 12, 15 with nine assumed wall thicknesses d_e = 0.1, 0.15, 0.2, 0.25, 0.3, 0.35, 0.4, 0.45, 0.5 m, are indicated in Figure 8. The same conclusions are drawn that the two target images simultaneously approach the center of antenna array to form two approximate linear traces with increasing assumed wall thickness and both two traces pass through their corresponding target true positions.

Two linear trajectories are fitted by using Radon transform for each image of Figure 8. Table 3 shows two groups of cross points from these linear trajectories for the two targets. The statistical means (−0.99 m, 3.01 m) and (1.93 m, 1.00 m) can be the effective estimations of target positions (−1.0 m, 3.0 m) and (2.0 m, 1.0 m). Then two estimated parameter pairs $(\hat{\varepsilon}, \hat{d})$ = (12, 0.212 m) and $(\hat{\varepsilon}, \hat{d})$ = (9, 0.226 m) are obtained for the two targets. As shown in Figures 9(a) and (b), the imaging results with the two estimated wall

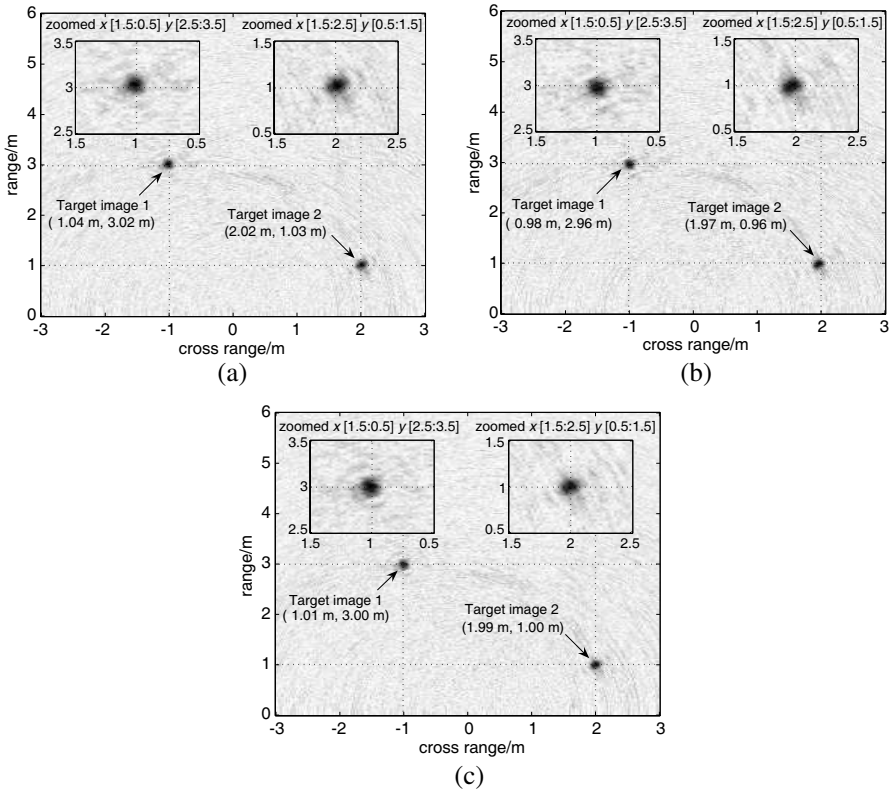

Figure 9. Imaging results with (a) $(\hat{\varepsilon}, \hat{d}) = (12, 0.212\,\text{m})$, (b) $(\hat{\varepsilon}, \hat{d}) = (9, 0.226\,\text{m})$, (c) $(\varepsilon_T, d_T) = (8.6, 0.24\,\text{m})$.

parameter pairs have the NSSIs with 3.68×10^{-14} and 3.75×10^{-14}, which is approximate to Figure 9(c) with the true wall parameters with 3.88×10^{-14} NSSI. Furthermore, the positions of target images in Figures 9(a) and (b) are compared with that in Figure 9(c) to indicate the approximate displacements of target images. Due to Figure 9(c) as the comparison criterion, it is demonstrated that these two pairs of estimated wall parameters can be used to generate the high-quality images.

On the condition of multi-targets, the sequences of target images are overlapping due to the small interval among these targets, as shown in Figure 10(b), which introduces interference errors in the linear trajectories fitted by Radon transform to generate bad localization results. In this case, the proposed approach can't resolve these targets. Now, resolution characteristic of this approach is considered by simulations. For simplicity of analysis, we focus on the simple case

of two point targets.

In the following simulation, the true wall relative permittivity $\varepsilon = 8.6$ with the nine assumed wall thicknesses $d_e = 0.1$, 0.15, 0.2, 0.25, 0.3, 0.35, 0.4, 0.45, 0.5 m is used. Other simulation setups are maintained except the positions of two point targets.

(i) When two targets pile up horizontally.
Figure 10(a) shows the simulation result with two targets locating at eight positions separately, where they pile up horizontally with the spacing 0.5 m. It is demonstrated that the resolution in image sequences becomes better when the two targets go away from the antenna array at the range direction, but gets worse with the two targets leaving the center of antenna array at the cross range direction. Generally, the spacing 0.5 m is available to separate the two image sequences.

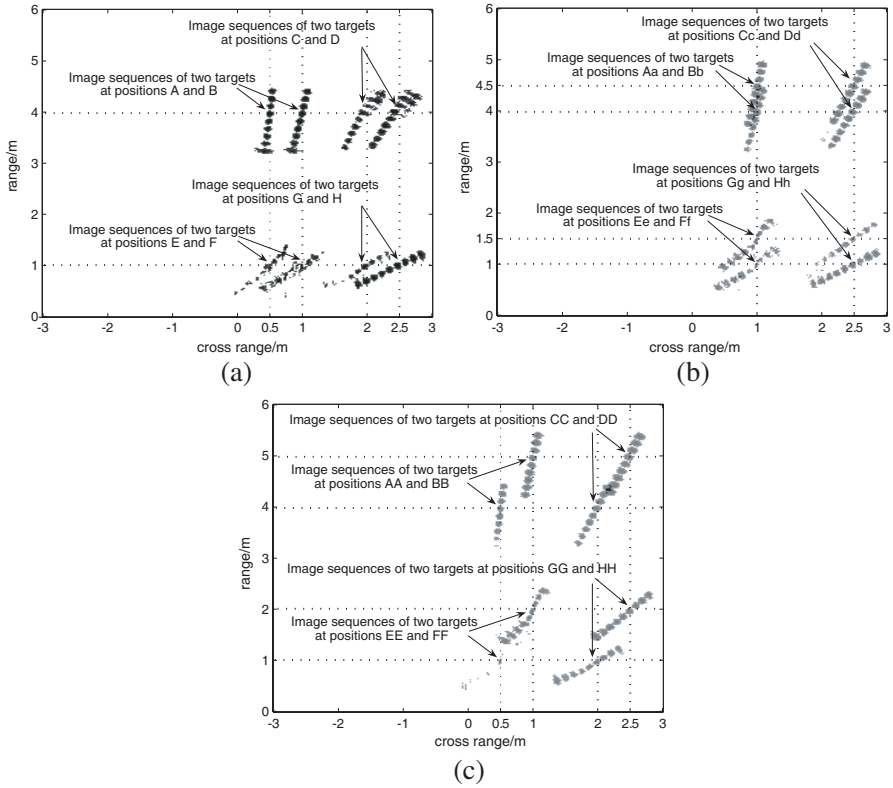

Figure 10. Image sequences of two targets when two targets pile up (a) horizontally, (b) vertically, (c) slantingly.

(ii) When two targets pile up vertically.
Based on the simulation result with two targets placed vertically at eight positions and the target spacing 0.5 m, as shown in Figure 10(b), the reverse conclusions are obtained. That is, with the two targets being away from the antenna array at the range direction, the resolution in image sequences gets worse, but the resolution becomes better when the two targets leave the center of antenna array at the cross range direction. In general, the spacing 0.5 m is fit for discriminating the two image sequences at the most of target locations.

(iii) When two targets pile up slantingly.
In this simulation, two targets slantingly pile up at eight positions with the distance 0.5 m in cross range and the distance 1 m in range. According to Figure 10(c), two image sequences have more overlap with the two targets being close to the same propagation path from the center of antenna array to one of the two targets.

The above simulation conclusions can be applied to the case of multi-targets. Besides, depending on the simulation results, the defocusing of target image becomes worse when the target is near to the center of antenna array, which exacerbates the interference between two targets. Thus, the proposed approach is not very practical for the case that multiple adjacent targets are close to the center of antenna array.

5. EXPERIMENT RESULTS USING STEPPED-FREQUENCY THROUGH-THE-WALL RADAR

In the collected echoes of synthetic aperture TWRI, the strong wall echoes, fully or partially overlapping the echoes of the close-to-wall target, can not be efficiently removed due to their fluctuation caused by non-uniform wall [19]. Consequently, an equivalent near-field wideband inverse synthetic aperture TWRI experiment has been set up in an empty room to verify the proposed approach. A stepped-frequency continuous wave signal, covering the band 1–2 GHz to provide good penetration capability through ordinary walls, is chosen for imaging in our through-the-wall radar system. The wall parameters are measured as $(\varepsilon,\, d) = (8.6,\, 0.28\,\mathrm{m})$ which are used as the true wall parameters in this paper, namely, $(\varepsilon_T,\, d_T) = (8.6,\, 0.28\,\mathrm{m})$.

Acting as one transmitter and one receiver, two dielectric antennas are fixed against the wall at the positions $(x,\, y) = (-0.25\,\mathrm{m}, -0.28\,\mathrm{m})$ and $(x,\, y) = (0.25\,\mathrm{m}, -0.28\,\mathrm{m})$. One person locates at 31 positions moving along with the horizontal line $y = 3\,\mathrm{m}$ with $x = [-2.1\,\mathrm{m} \sim 0.9\,\mathrm{m}]$ to implement inverse synthetic aperture imaging. That is to say,

the spacing of the adjacent person positions is 0.1 m. Therefore, the two antenna positions of the equivalent synthetic aperture array are listed in Table 4, and the equivalent person position is $(x, y) = (0.6\,\text{m}, 3.0\,\text{m})$. Figure 11 shows the geometry of the experiment scene with one person, and the relative parameters have been indicated. Besides, the heights of the room and human are 4 m and 170 m respectively, and the vertical coordinate of antenna array is 1.1 m. The imaging scene $x \times y = [-3\,\text{m} \sim 3\,\text{m}] \times [0\,\text{m} \sim 7\,\text{m}]$ is divided into 120×140 cells. In other words, each image consists of 120×140 pixels, where each pixel is a square of size 0.05 m.

Firstly, range profile plane is obtained by inverse Fourier transform for the measured stepped-frequency data from the receiving antenna array. The stationary clutters, such as wall echo and antenna coupling, do not allow the response of human target to be detected. In this paper, mean background subtraction technique is used to reject these stationary clutters. This technique is carried out on the range profile

Table 4. The transmitter and receiver locations of the equivalent synthetic aperture array.

Element ♯	1	2	3	...	29	30	31
Transmitter (m)	−1.75	−1.65	−1.55	...	1.05	1.15	1.25
Receiver (m)	−1.25	−1.15	−1.05	...	1.55	1.65	1.75

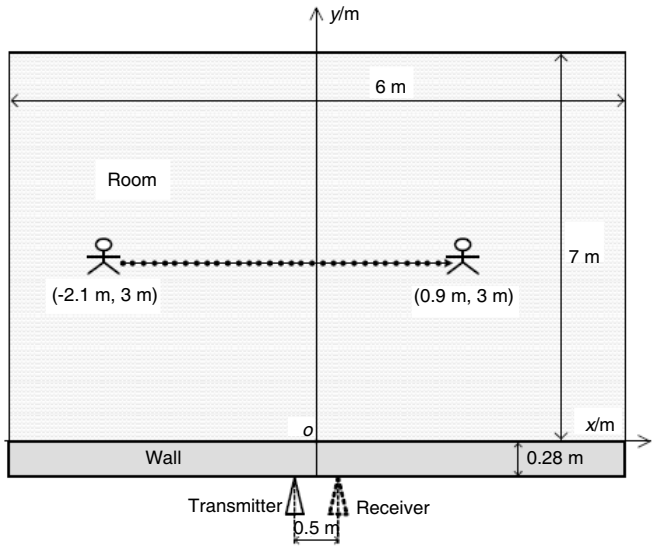

Figure 11. Geometry of the imaging scene with one human target.

plane by two steps. Firstly, the mean of all the range profiles is to serve as the estimated stationary clutters. Secondly, the estimated stationary clutters is subtracted from each range profile. After background subtraction, the range profile plane is used to form the image through back-projection imaging.

Figure 12 shows the results with four assumed relative permittivities $\varepsilon_e = 6$, 9, 12, 15 with nine wall thicknesses $d_e = 0.1$, 0.15, 0.2, 0.25, 0.3, 0.35, 0.4, 0.45, 0.5 m. Similar to the simulation results in Figure 4, along with the addition of assumed wall thickness, the target image moves toward the center of antenna array appearing an approximate linear trace to pass through the true target position. Through Radon transform, four fitted lines $y = k_n x + b_n$, $n = 1$, 2, 3, 4 are acquired in Figure 13. Because of the serious image defocusing in Figure 12, there are not the inverse relation between the slopes of four lines with fitted errors and the four relative permittivities. As

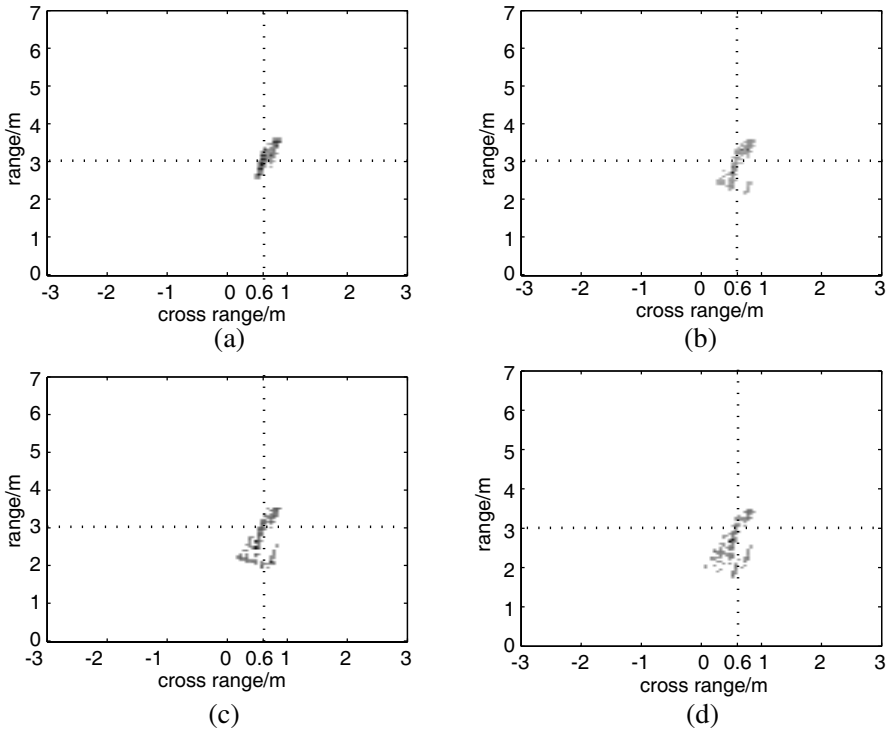

Figure 12. Image sequence of one person with $d_e = 0.1$, 0.15, 0.2, 0.25, 0.3, 0.35, 0.4, 0.45, 0.5 m for (a) $\varepsilon_e = 6$, (b) $\varepsilon_e = 9$, (c) $\varepsilon_e = 12$, (d) $\varepsilon_e = 15$.

a result, some cross points have bad fluctuation to be the estimated target positions, such as (0.80 m, 3.39 m) in Table 5. In order to weaken the fluctuation, the statistical mean (0.67 m, 3.05 m) of the $C_4^2 = 6$ intersections is used as the robust estimation of true human position (0.6 m, 3.0 m).

The estimation $\hat{\varepsilon} = 12$ of relative permittivity is found by step 5 and step 6, and the fitted first-order polynomial $d = A_3 y + B_3$ corresponding to $\hat{\varepsilon} = 12$ is shown in Figure 14. Then the estimation $\hat{d} = 0.243$ m of wall thickness is solved by $d = A_3\hat{y} + B_3$, $\hat{y} = 3.05$. Figure 15(a) is the image formed with the estimated wall parameters $(\hat{\varepsilon}, \hat{d}) = (12, 0.243\,\text{m})$, where there are 0.03 m displacement of target image and 9.05×10^{-12} NSSI. Similarly, Figure 15(b) with the true wall parameters $(\varepsilon_T, d_T) = (8.6, 0.28\,\text{m})$ is regarded as the

Table 5. Cross points of four fitted lines in Figure 12.

Combination of two ε_e	Cross point (x, y) of two corresponding linear trajectories
$\varepsilon_e = 6$ and $\varepsilon_e = 9$	(0.67 m, 3.04 m)
$\varepsilon_e = 6$ and $\varepsilon_e = 12$	(0.77 m, 3.31 m)
$\varepsilon_e = 6$ and $\varepsilon_e = 15$	(0.58 m, 2.80 m)
$\varepsilon_e = 9$ and $\varepsilon_e = 12$	(0.80 m, 3.39 m)
$\varepsilon_e = 9$ and $\varepsilon_e = 15$	(0.58 m, 2.82 m)
$\varepsilon_e = 12$ and $\varepsilon_e = 15$	(0.60 m, 2.95 m)
statistical mean $(\hat{x}, \hat{y})$	(0.67 m, 3.05 m)

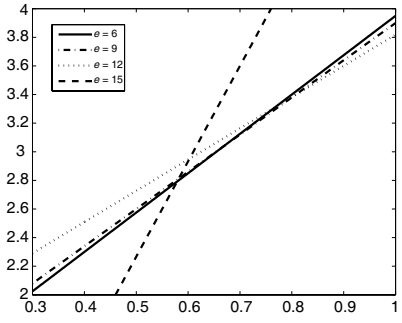

Figure 13. Four fitted lines with $\varepsilon_e = 6, 9, 12, 15$, $(\varepsilon_e = e)$.

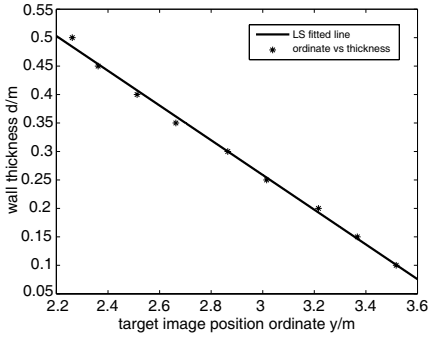

Figure 14. Least-square fitted polynomial with $\varepsilon_e = 12$.

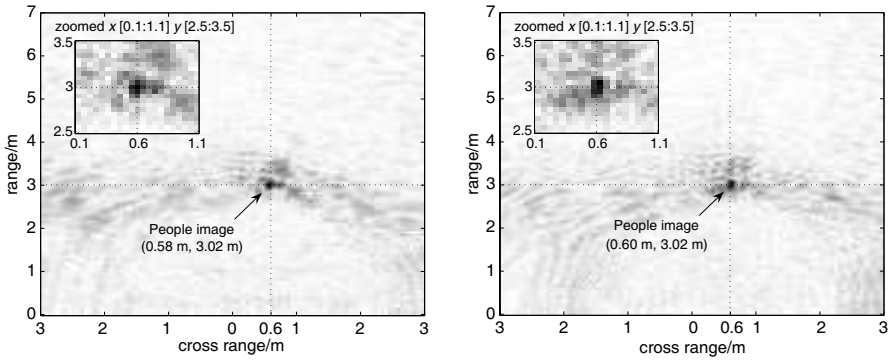

Figure 15. Imaging results with (a) $(\hat{\varepsilon},\, \hat{d}) = (12,\ 0.243\,\text{m})$, (b) $(\varepsilon_T = 8.6,\ d_T = 0.28\,\text{m})$.

comparison criterion, which has 0.02 m displacement of target image and 8.78×10^{-12} NSSI. Therefore, there are minor differences in the displacement of target image and NSSI, which demonstrates that the estimated wall parameters with errors can also be used to generate the high-quality image.

Then two persons with the equivalent positions $(-0.5\,\text{m},\ 2.5\,\text{m})$ and $(1.0\,\text{m},\ 3.0\,\text{m})$ move simultaneously to carry out inverse synthetic aperture imaging. Four image sequences for $\varepsilon_e = 6,\ 9,\ 12,\ 15$ with nine thicknesses $d_e = 0.1,\ 0.15,\ 0.2,\ 0.25,\ 0.3,\ 0.35,\ 0.4,\ 0.45,\ 0.5\,\text{m}$ are illustrated in Figure 16. With the addition of wall thickness, two target images come near to the center of antenna array together to form two approximate linear traces which pass through their corresponding target true positions.

Table 6 shows two groups of cross points from the linear displacement trajectories for the two targets. The statistical means $(-0.51\,\text{m},\ 2.54\,\text{m})$ and $(0.97\,\text{m},\ 2.98\,\text{m})$ are regarded as the effective estimations of target positions $(-0.5\,\text{m},\ 2.5\,\text{m})$ and $(1.0\,\text{m},\ 3.0\,\text{m})$. Then two pairs of estimated wall parameters $(\hat{\varepsilon},\, \hat{d}) = (9,\ 0.257\,\text{m})$ and $(\hat{\varepsilon},\, \hat{d}) = (12,\ 0.246\,\text{m})$ for the two targets are obtained. Figures 17(a) and (b) with the estimated wall parameters are compared with Figure 17(c) with the true wall parameters to indicate that the two estimated wall parameters can be used to generate the high-quality images with minor image differences. Quantitatively, in Figures 17(a) and (b), the displacements of two target images are $[0.02\,\text{m},\ 0.02\,\text{m}]$ and $[0.06\,\text{m},\ 0.02\,\text{m}]$, and NSSIs of the two images are 3.41×10^{-12} and 3.63×10^{-12}. Accordingly, there are $[0.02\,\text{m},\ 0.02\,\text{m}]$ displacements of two target images and 3.51×10^{-12} NSSI in Figure 17(c).

Table 6. Cross points of the fitted lines for two human targets.

Combination of two ε_e	Cross points (x, y) of the corresponding linear trajectories
$\varepsilon_e = 6$ and $\varepsilon_e = 9$	(−0.51 m, 2.54 m) (1.09 m, 3.26 m)
$\varepsilon_e = 6$ and $\varepsilon_e = 12$	(−0.48 m, 2.49 m) (0.96 m, 2.94 m)
$\varepsilon_e = 6$ and $\varepsilon_e = 15$	(−0.53 m, 2.57 m) (0.93 m, 2.87 m)
$\varepsilon_e = 9$ and $\varepsilon_e = 12$	(−0.46 m, 2.46 m) (0.85 m, 2.74 m)
$\varepsilon_e = 9$ and $\varepsilon_e = 15$	(−0.53 m, 2.57 m) (1.03 m, 3.12 m)
$\varepsilon_e = 12$ and $\varepsilon_e = 15$	(−0.56 m, 2.61 m) (0.95 m, 2.92 m)
statistical mean $(\hat{x}, \hat{y})$	(−0.51 m, 2.54 m) (0.97 m, 2.98 m)

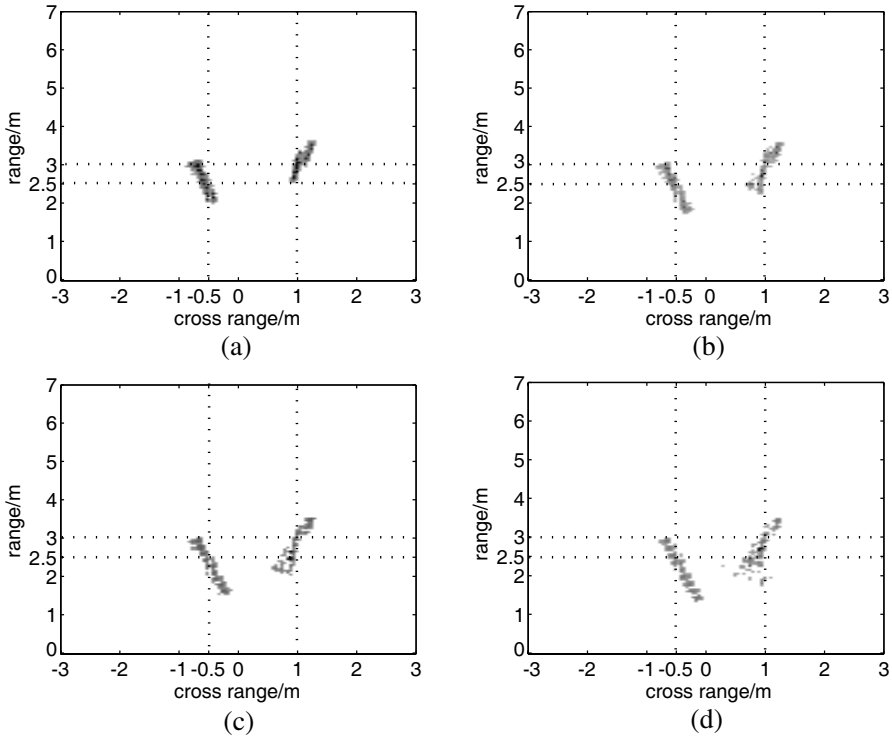

Figure 16. Image sequences of two persons with $d_e = 0.1$, 0.15, 0.2, 0.25, 0.3, 0.35, 0.4, 0.45, 0.5 m for (a) $\varepsilon_e = 6$, (b) $\varepsilon_e = 9$, (c) $\varepsilon_e = 12$, (d) $\varepsilon_e = 15$.

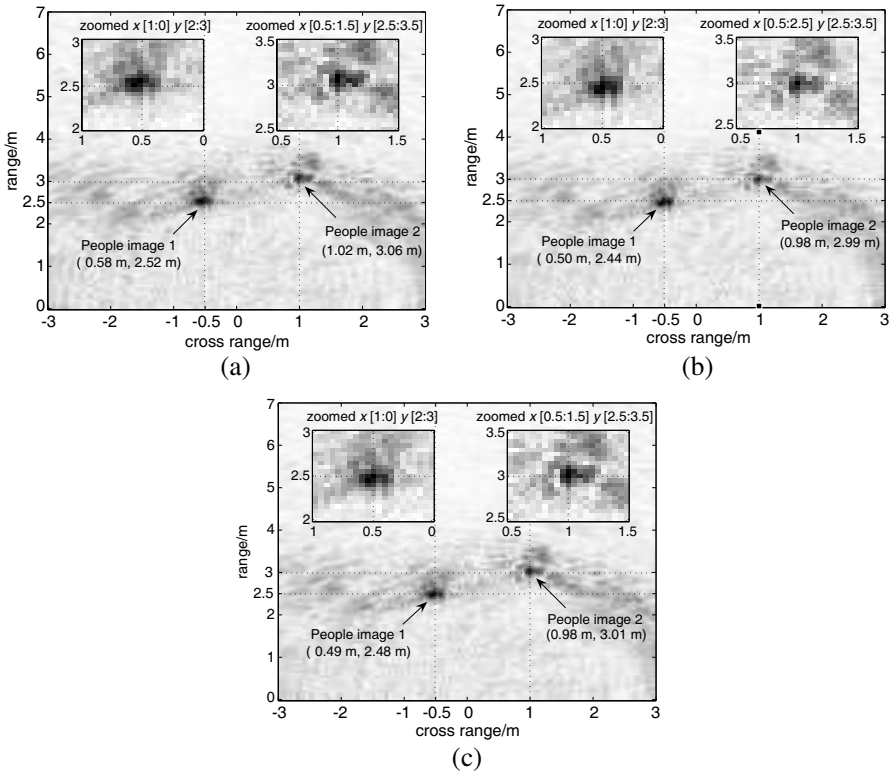

Figure 17. Imaging results with (a) $(\hat{\varepsilon},\, \hat{d}) = (9,\, 0.257\,\mathrm{m})$, (b) $(\hat{\varepsilon},\, \hat{d}) = (12,\, 0.246\,\mathrm{m})$, (c) $(\varepsilon_T, d_T) = (8.6,\, 0.28\,\mathrm{m})$.

6. CONCLUSION

In practical TWRI applications, errors in wall parameters cause target blurriness and displacement. In this paper, we have addressed a novel algorithm on the target localization with unknown wall parameters. The proposed approach obtains the estimated target position by searching the intersection of linear trajectories. These linear trajectories are fitted via Radon transform for the target image sequences corresponding to different assumed relative permittivities with different assumed wall thicknesses. Furthermore, the estimations of wall parameters are found to generate the high-quality images. The proposed approach is tested and verified by the simulation and experiment data. Compared with the two techniques in [17, 18], the approach does not need manual operations to change the setup of antenna array, which improves the potential localization accuracy and image quality, and ensures operator safety in practical applications.

ACKNOWLEDGMENT

This work was sponsored by National Natural Science Foundation of China (60802063) and by Sichuan Youth Science and Technology Foundation (2011JQ0024).

REFERENCES

1. Lu, T., K. Agarwal, Y. Zhong, and X. Chen, "Through-wall imaging: Application of subspace-based optimization method," *Progress In Electromagnetics Research*, Vol. 102, 351–366, 2010.
2. Ahmad, F., M. G. Amin, and S. A. Kassam, "Synthetic aperture beamformer for imaging through a dielectric wall," *IEEE Transactions on Aerospace and Electronic Systems*, Vol. 41, 271–283, 2005.
3. Yang, Y. Q. and A. E. Fathy, "See-through-wall imaging using ultra wideband short-pulse radar system," *IEEE AP-S International Symposium*, Vol. 3B, 334–337, Knoxville, United States, 2005.
4. Zheng, W., Z. Zhao, and Z.-P. Nie, "Application of TRM in the UWB through wall radar," *Progress In Electromagnetics Research*, Vol. 87, 279–296, 2008.
5. Ahmad, F., Y. M. Zhang, and M. G. Amin, "Three-dimensional wideband beamforming for imaging through a single wall," *IEEE Geoscience and Remote Sensing Letters*, Vol. 5, 176–179, 2008.
6. Soldovieri, F., R. Solimene, and R. Pierri, "A simple strategy to detect changes in through the wall imaging," *Progress In Electromagnetics Research M*, Vol. 7, 1–13, 2009.
7. Hantscher, S., A. Reisenzahn, and C. G. Diskus, "Through-wall imaging with a 3-D UWB SAR algorithm," *IEEE Signal Processing Letters*, Vol. 15, 269–272, 2008.
8. Zheng, W., Z. Zhao, Z.-P. Nie, and Q. H. Liu, "Evaluation of TRM in the complex through wall environment," *Porgress In Electromagnetics Research*, Vol. 90, 235–254, 2009.
9. Davy, M., T. Lepetit, J. de Rosny, C. Prada, and M. Fink, "Detection and imaging of human beings behind a wall using the DORT method," *Porgress In Electromagnetics Research*, Vol. 110, 356–369, 2010.
10. Zhang, W., A. Hoorfar, and L. Li, "Through-the-wall target localizaiton with time reversal music method," *Porgress In Electromagnetics Research*, Vol. 106, 75–89, 2010.
11. Cui, G. L., L. J. Kong, and J. Y. Yang, "A back-projection

algorithm to stepped-frequency synthetic aperture through-the-wall radar imaging," *1st Asian and Pacific Conference on Synthetic Aperture Radar Proceedings*, 123–126, 2007.

12. Kong, L. J., G. L. Cui, X. B. Yang, and J. Y. Yang, "Three-dimensional human imaging for through-the-wall radar," *IEEE 2009 Radar Conference*, 1–4, 2009.
13. Michal, A., S. Jurgen, D. Milos, and K. Dusan, "Efficient and fast method of wall parameter estimation by using UWB radar system," *Frequenz Journal*, 231–235, 2009.
14. Mandapati, G. and M. Amin, "Blurness and focusing-defocusing for through the wall radar imaging with wall ambiguities," *IEEE International Symposium on Signal Processing and Information Technology*, 246–249, 2004.
15. Amad, F., M. G. Amin, and G. Mandapati, "Autofocusing of through-the-wall radar imagery under unknown wall characteristics," *IEEE Transactions on Image Processing*, Vol. 16, 1785–1795, 2007.
16. Amad, F. and M. G. Amin, "Analyses of autofocusing schemes for indoor imaging with unknown walls," *IEEE Sensor Array and Multichannel Signal Processing Workshop Proceedings*, 358–362, 2006.
17. Wang, G. Y., M. G. Amin, and Y. Zhang, "New approach for target location in the presence of wall ambiguities," *IEEE Transactions on Aerospace and Electronic Systems*, Vol. 42, 301–315, 2006.
18. Wang, G. Y. and M. G. Amin, "Imaging through unknown walls using different standoff distances," *IEEE Transactions on Signal Processing*, Vol. 54, 4015–4025, 2006.
19. Amin, M. and H. Estephan, "An adaptive background estimation technique for enhancing target detection in through-the-wall-radar imaging applications," *Proceedings of SPIE — The International Society for Optical Engineering*, Vol. 7305, 2009.